Research Square

Preprints are preliminary reports that have not undergone peer review.
They should not be considered conclusive, used to inform clinical practice,
or referenced by the media as validated information.

Synthesis and Magnetic Properties of Novel 3d-4f Ln-Mn Hetero Nuclear Complexes

Fan Jiang
Liaoning Petrochemical University
Yue Ke
Liaoning Petrochemical University
Xiaohan Gao
Liaoning Petrochemical University
Yuchi Zhou
Liaoning Petrochemical University
Shuo Li
Liaoning Petrochemical University
Xuechuan Lv
xuechuanster@163.com
Liaoning Petrochemical University
Almas Tusipkhan
Karaganda Buketov University

Research Article

Keywords: 3d–4f Ln-TM hetero-metallic complexes, 2, 6-pyridine dicarboxylic acid, Single crystal, Antiferromagnetism, Spin-orbit coupling

Posted Date: August 20th, 2026

DOI: https://doi.org/10.21203/rs.3.rs-10641296/v1

License: This work is licensed under a Creative Commons Attribution 4.0 International License.
Read Full License

Additional Declarations: No competing interests reported.

Synthesis and Magnetic Properties of Novel 3*d*-4*f* Ln-Mn Hetero Nuclear Complexes

Fan Jiang[a], Yue Ke[a], Xiaohan Gao[a *], Yuchi Zhou[a], Shuo Li[a], Xuechuan Lv[b *], Almas Tusipkhan[c]

[a] *College of Petrochemical Engineering, Liaoning Petrochemical University, Liaoning Fushun, 113001, P.R.China*
[b] *College of Sciences, Liaoning Petrochemical University, Fushun 11300l, China*
[c] *Department of Chemical Technology and Petrochemistry, Buketov University, Karaganda, 100028, Kazakhstan*

**Corresponding author* E-mail: gaoxhan@163.com, xuechuanster@163.com

Abstract Single crystals of a family of 3*d*-4*f* Ln-Mn (Ln=lanthanide element) hetero nuclear bimetallic [Ln Mn] complexes $[Ln_2Mn(2,6\text{-dipic})_4(H_2O)_8]\cdot 10H_2O$ (Ln=La, Ce, Pr, Nd), (2, 6-dipic = pyridine-2, 6-dicarboxylic acid anion) were designed and synthesized. Unique novel structure of the complexes is a *Z*-shaped one-dimensional chain. In one unit, the carboxyl group (-COO) of the anion in pyridine dicarboxylic acid chelates one Ln^{3+} ion (*trans*) and one bridged Mn^{2+} ion (*cis*) in a *cis-trans* chelation mode, respectively. As a result, one Mn^{2+}ion connects two Ln^{3+} units in the form of a *cis-cis* bridge. The magnetic properties of the complexes were studied, the antiferromagnetic exchange interaction between adjacent paramagnetic ions was discovered. The magnetic data of the complexes were fitted using the Least Squares Method, and the estimated strength of the antiferromagnetic exchange interaction was obtained. At the same time, the spin orbit coupling phenomenon was explained.

Keywords: 3*d*–4*f* Ln-TM hetero-metallic complexes, 2, 6-pyridine dicarboxylic acid, Single crystal, Antiferromagnetism, Spin-orbit coupling

1. INTRODUCTION

Lanthanide transition metal (Ln-TM) bimetallic 3*d*-4*f* complexes have shown significant application value in fields such as biological imaging, magnetic materials, industrial catalysis, and anticancer drugs due to their unique electronic structure, magnetic characteristics, and photophysical properties[1-7]. These systems combine the rich electronic configurations and variable oxidation states of 3d metals with the unique magnetic anisotropy, strong spin-orbit coupling, and characteristic optical properties of 4f metals, giving rise to exceptional physical and chemical behaviors that are unattainable in homometallic counterparts. In recent years, 3*d*-4*f* hetero nuclear bimetallic magnetic materials have attracted great attention due to their enormous potential in high-density information storage devices, quantum computers, spintronics, and magnetocaloric materials[8-19].

In the field of coordination chemistry, for the high ground state spin value of transition metal ions themselves, introducing transition metal ions into rare earth complexes can enhance their magnetism. The orbital coupling between rare earth ions (4*f* electrons) and transition metals (3*d* electrons) can generate unique magnetic exchange interactions, forming complex magnetic ground states. In addition, the high coordination number 8-12 of rare earth ions can enhance the structural stability of complexes, making them suitable for multifunctional catalytic systems[20-22]. The structure and properties of ligands directly determine the spatial composition and application value of complexes.

Pyridine-2, 6-dicarboxylic acid, as a multifunctional ligand, combines the structural characteristics and performance advantages of both pyridine and carboxylic acid groups. The carboxyl oxygen atom can bind to metal ions through various coordination modes such as monodentate and bidentate. With strong coordination ability and multiple coordination modes, it not only endows the complexes with rich structural morphology, but also significantly enhances the stability of the framework[12-25]. The deprotonated partially or completely carboxyl groups allow the ligand to exist in different forms such as monovalent anions, divalent anions, or neutral molecules, resulting in diverse coordination configurations. In addition, the rigid structure endowed by the pyridine ring complements the rotatable and flexible orientation of the carboxyl group, enabling it to form porous polymers with regular topological structures. These advantages make pyridine-2, 6-dicarboxylic acid an ideal structural unit for constructing coordination polymers and play a key role in the synthesis of coordination compounds[26-32].

Our group have been studying mononuclear and binuclear metal complexes of the mixed dipic ligand[33]. Two heterometallic coordination polymers $H_3O[LnMn_2(2,6\text{-dipic})_3Ac_2(H_2O)_6]\cdot 3H_2O$ (Ln: Ho, Dy) were synthesized. Ln and Mn ions were inter linked by the oxygen atoms of pyridine-2, 6-dicarboxylic acid and acetic acid, forming a special semi-staggered network. The magnetic behaviors of the complexes were revealed. While in this work, a series of different complexes $[Ln_2Mn(2,6\text{-dipic})_4(H_2O)_8]\cdot 10H_2O$ (Ln=La, Ce, Pr, Nd) with a *Z*-shaped one-dimensional chain were reported. The magnetic properties and thermal stability of the complexes were studied. The structure- activity relationships in these complexes were explored.

2. EXPERIMENTAL

2.1 Physical measurements

The single crystal structure data of the complex was determined by a Smart 1000 X-ray single crystal diffractometer under the conditions of a tube voltage of 30 kV and a tube current of 100 mA. Fourier transform technique and SHELXL-97 program were used to analyze and refine the single crystal structure data. The temperature dependent magnetic susceptibility of the complexes was determined by quantum SQUVID-VSM, with a field strength of 1000 Oe and a measurement range of 2-300 K. Using a Fourier transform infrared spectrometer (Type Spectrum GX Fourier transform infrared spectrometer) Perkin Elmer Company collected IR absorption data of free ligands and complexes in the range of 4000-400 cm^{-1} using KBr pellets with a resolution of 2 cm^{-1} at room temperature. The DSC curves of the complexes were measured using a DSC-141 differential scanning calorimetry. Nitrogen was used as the protective gas, with a heating rate of 10 $K \cdot min^{-1}$ and a nitrogen flow rate of 50 $cm^3 \cdot min^{-1}$. The analysis temperature range was 300-800 K. The TG curves of the complex were measured by an SDT-Q600 thermogravimetric analyzer, with nitrogen as the protective gas, a flow rate of 50 $cm^3 \cdot min^{-1}$, a heating rate of 10 $K \cdot min^{-1}$, and an analysis temperature range of 300-1100 K. $CaC_2O_4 \cdot H_2O$ was used as the reference material and calibrated using SMR.

2.2 Synthesis of the complexes

All complexes $[Ln_2Mn(2, 6\text{-dipic})_4(H_2O)_8] \cdot 10H_2O$,(Ln=La, Ce, Pr, Nd,) were obtained using the same method. $Ln(NO_3)_3 \cdot 6H_2O$ (1 mmol), $MnCl_2 \cdot 4H_2O$ (1 mmol), 2, 6-pyridinedicarboxylic acid (2 mmol) were added to 20 mL of deionized water under magnetic stirring condition to obtain a clear solution respectively. NaOH solution (1 mol L^{-1}) was added to the two metal salt solutions until the precipitation point was reached. the pH value of the carboxylic acid solution was adjusted to about 8 by NaOH solution (1 mol L^{-1}). Two metal salt solutions were mixed, then the carboxylic acid solution was added dropwise and heated in a water bath at 90 °C for 1 hour. The above solution was filtered immediately and collected in a culture dish. After a few weeks, the colored crystals were obtained.

3 RESULTS AND DISCUSSION

3.1 Crystal structures of the complexes

The crystal structure formula of this complex family is $[Ln_2Mn(2, 6\text{-dipic})_4(H_2O)_8] \cdot 10H_2O$ (Ln=La, Ce, Pr, Nd). Given the high similarity in the structures of all family members, the complex $[Nd_2Mn(2, 6\text{-dipic})_4(H_2O)_8] \cdot 10H_2O$ is taken as an example for detailed structural analysis, and its characteristics can serve as a representative structural description of the entire series of complexes.

The structure of the complex $[Nd_2Mn(2, 6\text{-dipic})_4(H_2O)_8] \cdot 10H_2O$ is shown in Fig. 1. The coordination units of rare earth ion Nd^{3+} and transition metal ion Mn^{2+} were shown in Fig. 2. The stacking structure diagram of the complex along three directions (*a*, *b*, *c*) were shown in Fig. 3. The crystallographic data obtained from single crystal measurements of the complex were listed in Table 1. Other information, such as the selected key length and key angle of the

product, can be found in Tables 2. The data for the other complexes is provided in the Supporting Information (Tables S1-S3).

Table 1. Crystal data and structure of the four complexes [a,b,c]

	Ln = La	Ln = Ce	Ln = Pr	Ln = Nd
CCDC reference numbers	2444256	2444255	2444253	2444254
Empirical formula	$C_{28}H_{48}O_{35}N_4MnLa_2$	$C_{28}H_{40}O_{34}N_4MnCe_2$	$C_{28}H_{32}O_{32}N_4MnPr_2$	$C_{28}H_{44}O_{34}N_4MnNd_2$
Formula weight	1333.46	1311.20	1273.33	1328.12
Crystal system	monoclinic	monoclinic	monoclinic	monoclinic
Space group	*C 2/c*	*C 2/c*	*C 2/c*	*C 2/c*
a(Å)	25.410(11)	25.308(3)	25.2505(13)	25.2014(18)
b(Å)	16.023(6)	15.9335(15)	15.9194(7)	15.9037(11)
c(Å)	12.431(5)	12.4316(12)	12.3869(6)	12.3898(9)
α(°)	90	90	90	90
β(°)	96.095(14)	96.260(3)	96.417(2)	96.576(2)
γ(°)	90	90	90	90
Volume(Å^3)	5032(3)	4983.0(8)	4948.0(4)	4933.1(6)
Z	4	4	4	4
Dc (mg/m^3)	1.760	1.759	1.709	1.788
F(000)	2652.0	2628.0	2508.0	2644.0
Measured reflections	38204	11094	10878	22102
Independent reflections	4496	4399	4329	4356
Goodness of fit on F^2	1.026	1.087	1.090	1.054
Final *R* indices[$I>2\sigma(I)$]	[a]*R1* = 0.0614,	[a]*R1*= 0.0307,	[a]*R1*= 0.0487,	[a]*R1*= 0.0363,
	[b]*ωR2* = 0.1706	[b]*ωR2* = 0.0839	[b]*ωR2* = 0.1563	[b]*ωR2* = 0.0963
R indices(all data)	[a]*R1* = 0.0835,	[a]*R1*= 0.0369,	[a]*R1*= 0.0647,	[a]*R1*= 0.0425,
	[b]*ωR2* = 0.2051	[b]*ωR2* = 0.0879	[b]*ωR2* = 0.1716	[b]*ωR2* = 0.1015

[a] $R = \sum \| F_o | - | F_c \| / \sum | F_o |$.

[b] $R_w = \left\{ \sum w[(|F_o|^2 - |F_c|^2)^2] / \sum w[(|F_o|^2)^2] \right\}^{1/2}$

[c] Estimated standard deviations in the last significant digits were given in parentheses.

Table 2. Selected bond lengths [Å] and angles [°] of Nd complex

Selected bond lengths [Å] of $[Nd_2Co(2, 6\text{-dipic})_4(H_2O)_8]\cdot 10H_2O$					
Nd1-O1	2.514(3)	Nd1-O5	2.507(3)	Nd1-O10	2.492(3)
Nd1-O1[1]	2.532(3)	Nd1-O7	2.462(3)	Nd1-N1	2.570(4)
Nd1-O3	2.482(3)	Nd1-O9	2.549(3)	Nd1-N2	2.578(4)
Selected bond angles [°] of $[Nd_2Mn(2, 6\text{-dipic})_4(H_2O)_8]\cdot 10H_2O$					
O1-Nd1-O9	79.65(11)	O3-Nd1-O9	133.23(12)	O7-Nd1-N1	135.81(12)
O1-Nd1-N1	62.59(11)	O3-Nd1-N1	62.89(12)	O7-Nd1-N2	63.01(12)
O1-Nd1-N2	134.01(12)	O3-Nd1-N2	70.36(12)	O9-Nd1-N1	119.97(12)
O3-Nd1-O1	125.33(11)	O5-Nd1-O1	76.35(11)	O9-Nd1-N2	123.54(12)
O3-Nd1-O5	82.54(12)	O5-Nd1-N1	70.57(12)	O10-Nd1-O1	90.91(12)
O3-Nd1-O9	133.23(12)	O5-Nd1-N2	62.35(12)	O12-Mn1-O8	87.94(17)
O3-Nd1-O10	73.59(12)	O7-Nd1-O1	152.74(11)	O12-Mn1-O11	92.70(18)
O3-Nd1-O1	125.33(11)	O7-Nd1-O5	125.32(11)	C14-O8-Mn1	122.8(3)
O3-Nd1-O5	82.54(12)	O7-Nd1-O10	81.64(12)	C6-O1-Nd1	124.9(3)

Note: i Represents the position (11/2-X,3/2-Y,1-Z).

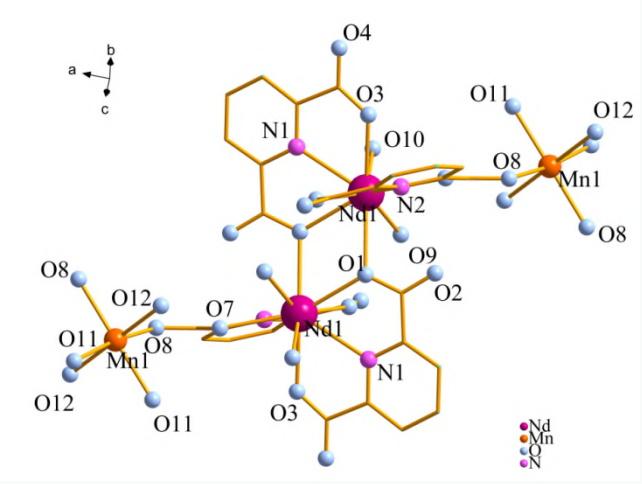
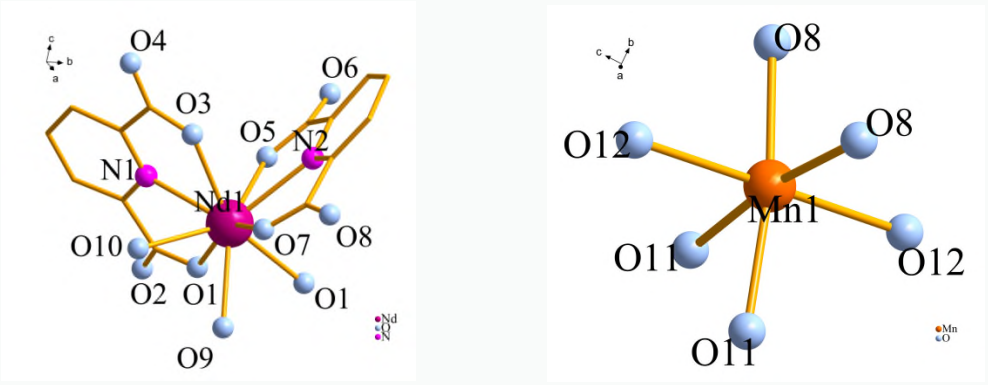


Fig.. 1 Crystal structure of $[Nd_2Mn(2, 6\text{-dipic})_4(H_2O)_8]\cdot 8H_2O$. Due to the structural similarity of all complexes, a detailed description of the structure of the complex (Ln = Nd) were considered as a representative structure of the whole family.



(a) (b)

Fig. 2 (a) Coordination unit of the rare earth ion Nd^{3+} (b) Coordination unit of transition metal ion Mn^{2+}

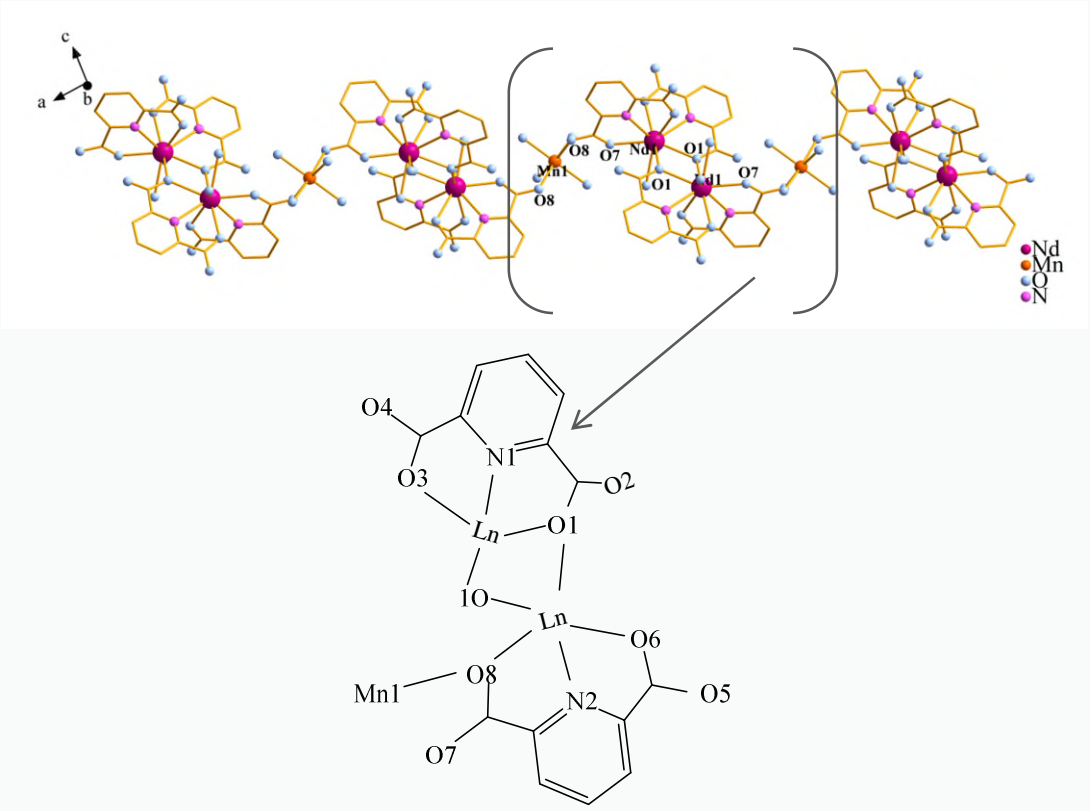


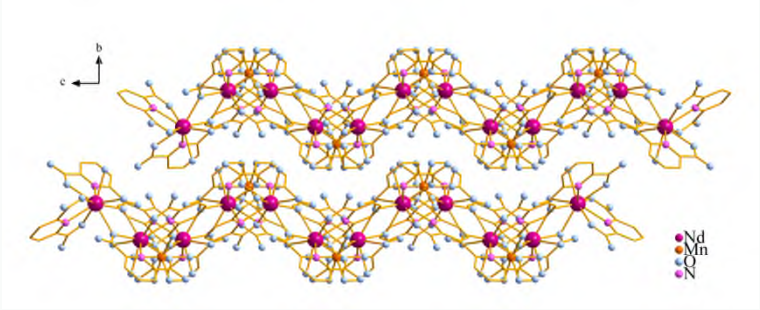
Fig. 3. Coordination mode 2, 6-pyridyldicarboxylic acid with Nd^{3+} and Mn^{2+}

The molecular structure of the complex $[Nd_2Mn(2, 6\text{-dipic})_4(H_2O)_8]\cdot 10H_2O$ was shown in Fig. 1. This complex belongs to the *C*2/*c* space group of the monoclinic crystal system. Each coordination unit consists of two rare earth ions Ln^{3+}, one transition ion Mn^{2+}, four 2,6-pyridinedicarboxylic acid anions, and eight coordinated water molecules.

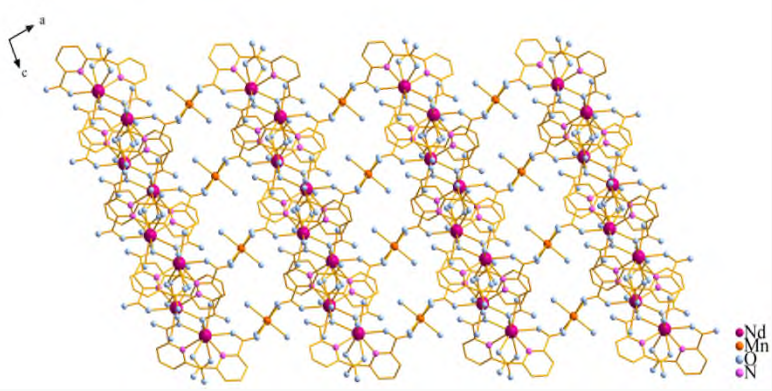
Each Ln^{3+} center is in a nine-coordinate environment and surrounded by five oxygen atoms from three ligands, two nitrogen atoms from two ligands and, two oxygen atoms from two coordinated water molecules. The bond lengths of two tridentate chelating ligands (O1, N1, O3) and two pyridine-2,6-dicarboxylic acid anions (O5, N2, O7) were Nd1-N1 [2.514(3)°],

Nd1-N2 [2.578(4)°], and the bond angles were N1-Nd1-N2 [116.20(12)°], O1-Nd1-O3 [125.33(11)°], and O7-Nd1-O5 [125.32(11) °], respectively, as shown in Fig. 2 (a) and Fig. 3. Two O (O9, O10) in H_2O coordinate with Ln^{3+}ions. Another O11 comes from the carbonyl group of another pyridine-2,6-dicarboxylic acid anion, coordinated with adjacent Ln^{3+} ions, with bond angles of O1-Nd1-O1 [65.66(13)°] and Nd1-O1-Nd1 [114.34(13)°], showing O1-Nd1-O1-Nd1 (μ_2:η^2:μ_2:η^2).

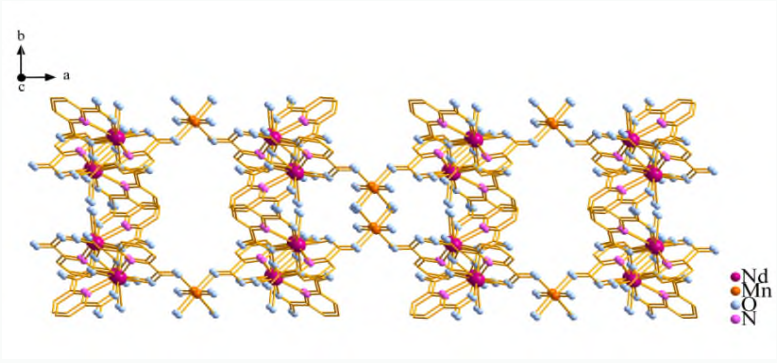
Each Mn^{2+}($3d^5$) ion is in a six-coordinate environment and surrounded by six oxygen atoms, forming an octahedral unit-*cis*-[$Mn(H_2O)_4(COO)_2$]. Four H_2O (two O11 and two O12) and two COO^- (two O8) of two pyridine-2,6-dicarboxylic acid anions coordinate with one Mn^{2+}, with bond angles of O8-Mn1-O8 [95.4(2)°], O8-Mn1-O12 [87.94(17)°], and O12-Mn1-O12 [179.8(3)°], respectively. Two O atoms along the same side of a squwere (cis). One Mn^{2+} forms a *cis-cis* carboxyl bridge conformation (-Ln$^{\underline{anti}}$O7-O8$^{\underline{syn}}$Mn$^{\underline{syn}}$O8-O7$^{\underline{anti}}$Ln-), with Mn^{2+} serving as the center of the conformational chain, as shown in Fig. 3 (b). According to crystal field theory, ligands COO- and H_2O were weak field ligands. When the ligands COO- and H_2O coordinate with Mn^{2+} ($3d^5$) ions, the crystal field splitting energy (Δ) is less than the pairing energy (P) , forming a high spin complex.



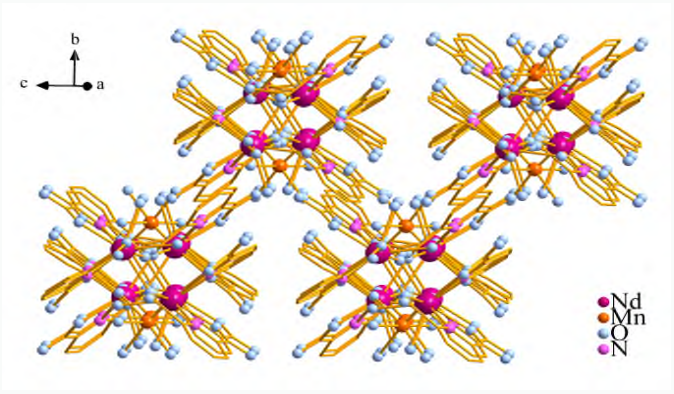
(a)



(b)



(c)



(d)

Fig. 4 The packing diagrams of $[Nd_2Mn(2, 6\text{-dipic})_4(H_2O)_8]\cdot 10H_2O$ from *a* (a) *b* (b) and *c* (c) direction and along the direction of the chain, which show the parallel of coordinating pyridine-2, 6-dicarboxylic acid anion (d).

The stacking diagrams of the complexes from four different directions were shown in Fig. 4, which shows that the complex $[Nd_2Mn(2,6\text{-dipic})_4(H_2O)_8]\cdot 10H_2O$ is stacked along a *Z*-shaped chain. Two pyridine-2, 6-dicarboxylic acid ligands and one Ln^{3+} ion were parallel to the direction of the chain (Fig. 2 (a) and Fig. 4 (d)). Fig. 4 (d) shows the parallel coordination of pyridine-2, 6-dicarboxylic acid along the chain, which is beneficial for the stability of the complex structure[33].

3.2 Magnetic properties

The magnetic properties of four series of similar complexes were studied, and the molar absorptions of the four complexes (Ln=La, Ce, Pr, Nd) at temperature (χ_M-T, $\chi_M T$-T and $1/\chi_M$-T) were plotted in Fig. 5 (La), (Ce), (Pr) and (Nd), respectively.

Taking Ln = Nd^{3+} as an example, in Fig. 5 (Nd). From the χ_M curve in Fig. 5 (Nd), it can be seen that when the temperature decreases from 300 K to 25 K, the χ_M value increases from 0.0283 $cm^3\,mol^{-1}$ to 0.239 $cm^3\,mol^{-1}$. As the temperature continues to decrease, the value of χ_M increases rapidly. When the temperature decreases to 5.4 K, the χ_M value reaches its maximum value of 0.996 $cm^3\,mol^{-1}$. The increase in molar magnetization with decreasing temperature indicates a lack of long-range ordering in spin and no anomalies.

Fig. 5 (Nd) shows that the molar magnetic susceptibility $\chi_M T$ increases steadily with decreasing temperature.The decrease in $\chi_M T$ value from 300 to 50 K is very slow, and when the temperature reaches 2.0 K, its value reaches 9.9 $cm^3\cdot K\cdot mol^{-1}$. For a free Nd^{3+} ion (J=(9/2),

S=3/2, *L*=6, *g*=8/11, μ_{eff} = 3.62 B. M) and a free Mn^{2+} center (*S*=5/2, *L*=0, *g*=2, μ_{eff}=5.92 B.M), the expected effective magnetic moment is 6.93 B. M).($\mu_{eff}=\sqrt{\mu^2_{eff(Nd^{3+})}+\mu^2_{eff(Mn^{2+})}}$).Fig. 5 (b) shows that at a temperature of 300 K, the $\chi_M T$ product of the complex $Nd^{3+}$is 8.488 $cm^3 \cdot K \cdot mol^{-1}$. The calculated effective magnetic moment μ_{eff} is 8.239 B.M, ($\mu_{eff}=2.828\sqrt{\chi_M T}$), which is consistent with the expected value.

In Fig. 5 (1), the variation of $1/\chi_M$ with complex *T* is linearly fitted using Curie Weiss law from 50 to 300 K, with $\chi = C/(T-\theta)$ (1). The effective magnetic moment, Curie constant (*C*), and Weiss temperature (θ) of four complexes were calculated and listed in Table 3. The negative value of Weiss temperature (θ) indicates a widespread antiferromagnetic correlation between spins [34, 35]. For the complex (Ln=Nd^{3+}), within the temperature range of 310 K (8.389 $cm^3 \cdot K \cdot mol^{-1}$) to 5.4 K (5.420 $cm^3 \cdot K \cdot mol^{-1}$), the value of $\chi_M T$ shows a continuous decreasing trend with temperature, and the value of Weiss temperature is always negative. This means that even in zero field, a spontaneous moment at finite temperature will be formed. Both phenomena can be explained by antiferromagnetic exchange and spin orbit coupling effects.

To estimate the strength of the antiferromagnetic effect, we used the following nonlinear equation (2) and least squweres optimization method to fit the $\chi_M T$ value, and the results were summarized in Table 2. Among them, $A_1+A_2=C$ (where *C* is the Curie constant), E_1 and E_2 correspond to the activation energies of spin-orbit coupling and antiferromagnetic exchange, respectively[36]. This equation well describes spin-orbit coupling; This coupling leads to the splitting between discrete energy levels and the exponential low-temperature divergence of magnetization[37].

$$\chi_M T = A_1 \exp\left(-\frac{E1}{kT}\right) + A_2 \exp\left(-\frac{E2}{kT}\right) \qquad (2)$$

In the high temperature range, the value of *C* is consistent with the value obtained according to Curie-Weiss law, (table 4) while the value of E_1/k is consistent with the spin orbit coupling effect and position distortion (E_1/k is on the order of 100 K) given in the literature [38]. When $Mn^{2+}(3d^5)$ coordinates with weak field ligands COO- and H_2O, an octahedral *cis* structural group *cis*-[$Mn(H_2O)_4(COO)_2$] is formed. Due to their weak field ligands, COO- and H_2O only undergo small crystal field splitting. The crystal field splitting energy (Δ) of COO- and H_2O is lower than the pairing energy (*P*) of Mn^{2+}, $\Delta<P$. It can be inferred that all four complexes (Ln=La, Ce, Pr, Nd,) were high spin complexes.

In Mn^{2+} centered carboxylic acid bridged complexes, the exchange coupling strength is closely related to the conformation of the carboxyl bridge. The *syn-syn* carboxyl bridge conformation (-Ln^{anti}O1-O2^{syn}Mn^{syn}O2-O1^{anti}Ln-) corresponds to strong antiferromagnetic coupling, while the *syn-anti* conformation (-Mn^{syn}O2-O1^{anti}Ln-) corresponds to weak antiferromagnetic coupling. In both conformations, antiferromagnetic coupling is transmitted through carboxyl bridges. Current research has shown that antiferromagnetic exchange coupling is commonly present in such complex chains, and the strength difference is essentially due to the regulation of electron delocalization pathways by carboxyl bridge conformation[39].

According to formula (3) and in combination with Julius' rule,where z is the number of newerest neighbors, S is the spin value and J (single J format) is the newerest-neighbor exchange strength. For the antiferromagnetic Mn^{2+} (S=5/2) chains that had two newerest neighbors (z=2) yielded J/k_B = –3.39 K (for Nd^{3+} complex). The magnetic exchange constant is negative (J<0), and there is antiferromagnetic coupling between $Mn^{2+}$and Ln^{3+}. The absolute value of J is relatively small, indicating that the two metal centers form weak antiferromagnetic coupling through bridging ligands. This is because the linear arrangement of metal ligand metal in the *syn-anti* structure weakens orbital overlap, leading to a significant reduction in exchange interaction.

$$\theta(S)=\frac{zS(S+1)J}{3k_B} \quad (3)$$

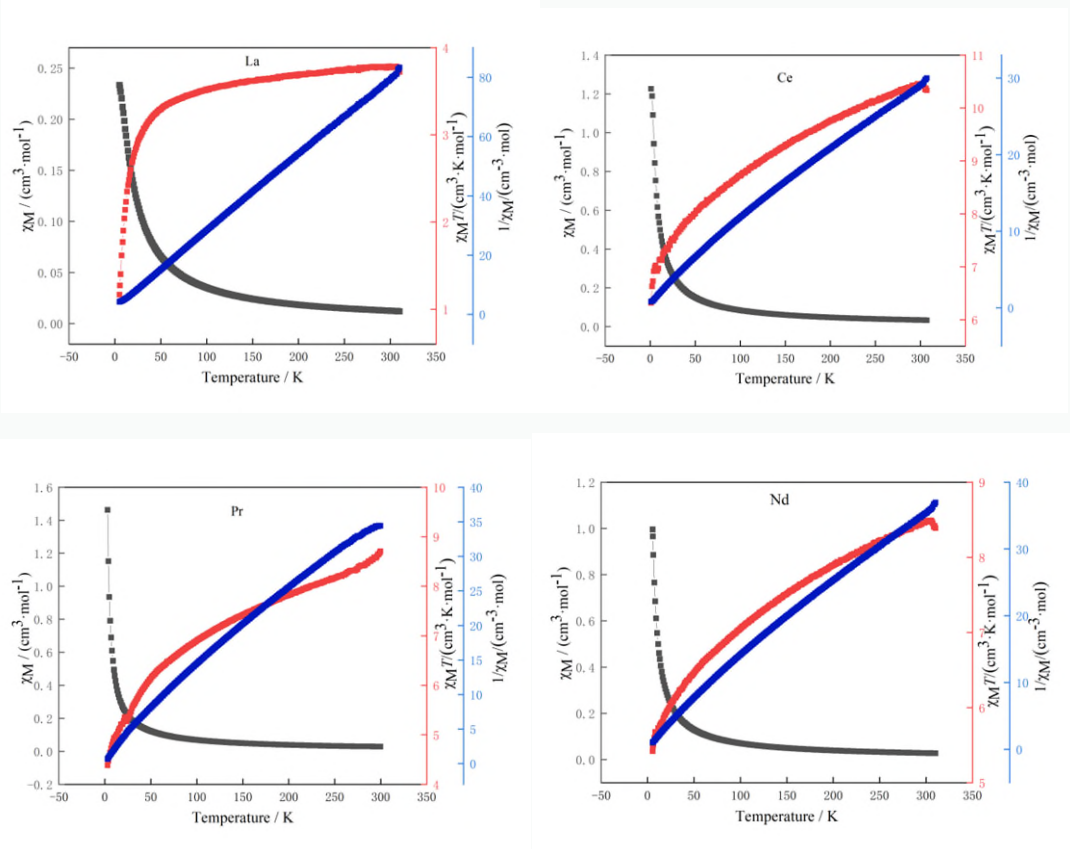


Fig.. 5 (a) The (χ_M-T), ($\chi_M T$-T), ($1/\chi_M$-T), curves of the $[Ln_2Mn(2,6\text{-dipic})_4(H_2O)_8]\cdot 10H_2O$, Ln=La，Ce，Pr，Nd.

Table 4. Different parameters obtained from the fitting of the magnetic data for the complexes.

Complexes	C	Θ	A_1+A_2	A_1	E_1/k	A_2	E_2/k
	$cm^3\cdot K\cdot mol^{-1}$	K			K		K
$Ln=La^{3+}$	3.89	-9.95	4.10	0.38	305.50	3.72	6.09
$Ln=Ce^{3+}$	10.84	-19.78	12.18	4.25	159.60	7.90	1.17
$Ln=Pr^{3+}$	8.88	-23.17	9.59	3.93	109.98	5.66	1.09
$Ln=Nd^{3+}$	8.81	-19.78	9.84	3.46	156.68	6.38	1.06

3.3 Infrared spectrum analysis

The infrared spectra of the complex $[Ln_2Mn(2,6\text{-dipic})_4(H_2O)_8]\cdot 10H_2O$ and ligand 2, 6-dicarboxylic acid were shown in Fig. 6, and the characteristic absorption peaks of the free ligand and the complex were shown in Table 5. The strong peak near 3411 cm^{-1} in Fig. 6 comes from the stretching vibration of O-H in the coordinated water and free water[40]. As shown in Fig. 6, the strong absorption peak of the ligand at 1700 cm^{-1} is attributed to the C=O stretching vibration of free carboxyl groups. This peak completely disappears in the complex, while new strong absorption bands emerge at 1614 cm^{-1} and 1578 cm^{-1}, which are assigned to the asymmetric stretching vibration of carboxylate groups ($\nu_{as}(COO^-)$). The intense peaks at 1431 cm^{-1} and 1387 cm^{-1} correspond to the symmetric stretching vibration of carboxylate groups ($\nu_s(COO^-)$), demonstrating that the ligand is fully deprotonated and coordinates with metal ions Mn^{2+} and Nd^{3+}. The wavenumber difference ($\Delta\nu$) between the asymmetric and symmetric stretching vibrations of carboxylate is less than 200 cm^{-1}, revealing that the carboxylate groups of the 2,6-$dipic^{2-}$ ligand coordinate with Nd^{3+}/Mn^{2+} via a bidentate bridging mode, and there exist two distinct coordination modes for the carboxylate anions in the ligand[41]. The presence of weak band around 527 and 432 cm^{-1} can be assigned to the stretching vibration of the Ln–N bond and Ln–O bond.

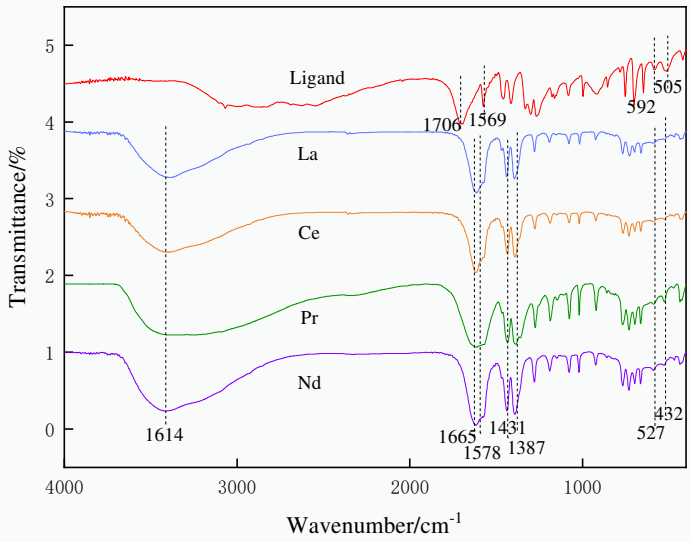


Fig. 6 The IR spectrum of the complexes $[Ln_2Mn(2, 6\text{-dipic})_4(H_2O)_8]\cdot 10H_2O$ and ligand 2, 6-dicarboxylic acid

Table 5. The characteristic peaks of the free ligand and the complexes.

Compound	absorption band		band assignment	absorption band		band assignment	Δν1	Δν2
H_2dipic	1706		υ(C=O)	1267		υ(C-O)		
$Ln=La^{3+}$	1618	1574	$\upsilon_{as}(COO^-)$	1438	1388	$\upsilon_s(COO^-)$	180	186
$Ln=Ce^{3+}$	1622	1570	$\upsilon_{as}(COO^-)$	1437	1394	$\upsilon_s(COO^-)$	185	176
$Ln=Pr^{3+}$	1620	1565	$\upsilon_{as}(COO^-)$	1435	1387	$\upsilon_s(COO^-)$	185	178
$Ln=Nd^{3+}$	1614	1578	$\upsilon_{as}(COO^-)$	1431	1387	$\upsilon_s(COO^-)$	183	191

3.4 Thermal stabilities

The DSC and TG curves of the complexes were shown in the Fig. 7. Due to the similar thermal behavior of the four complexes, taking Ln=Ce^{3+} Fig. 7 as an example. The mechanism of compound decomposition can be mainly divided to be two stages.

In Fig. 7(Ce), from 303 to 445 K, there were two endothermic peaks in the DSC curve, and the TG curve can be divided into two small stages, which due to the loss of the 10 free water molecules and the 4 coordinated water molecules, respectively, with a total weight loss ratio of 22.47% (theoretical value is 24.57 %).

From 445-1015 K, there was a large exothermic peak (2) attributed to the decomposition of the ligand pyridine skeleton. While the TG curve had one big stage, 26.45% (theoretical value: 26.54%), which due to the breakage of C-O and C-N bonds. The final products were inferred to be Ce_2O_3, MnO and C.

$$[Ce_2Mn(2,6\text{-dipic})_4(H_2O)_8]\cdot 10H_2O \xrightarrow[22.47\%(24.57\%)]{303\sim 445K} [Ce_2Mn(2,6\text{-dipic})_4]$$

$$[Ce_2Mn(2,6\text{-dipic})_4] \xrightarrow[26.45\%(26.45\%)]{445\sim 1085K} Ce_2O_3\text{ , MnO and C}$$

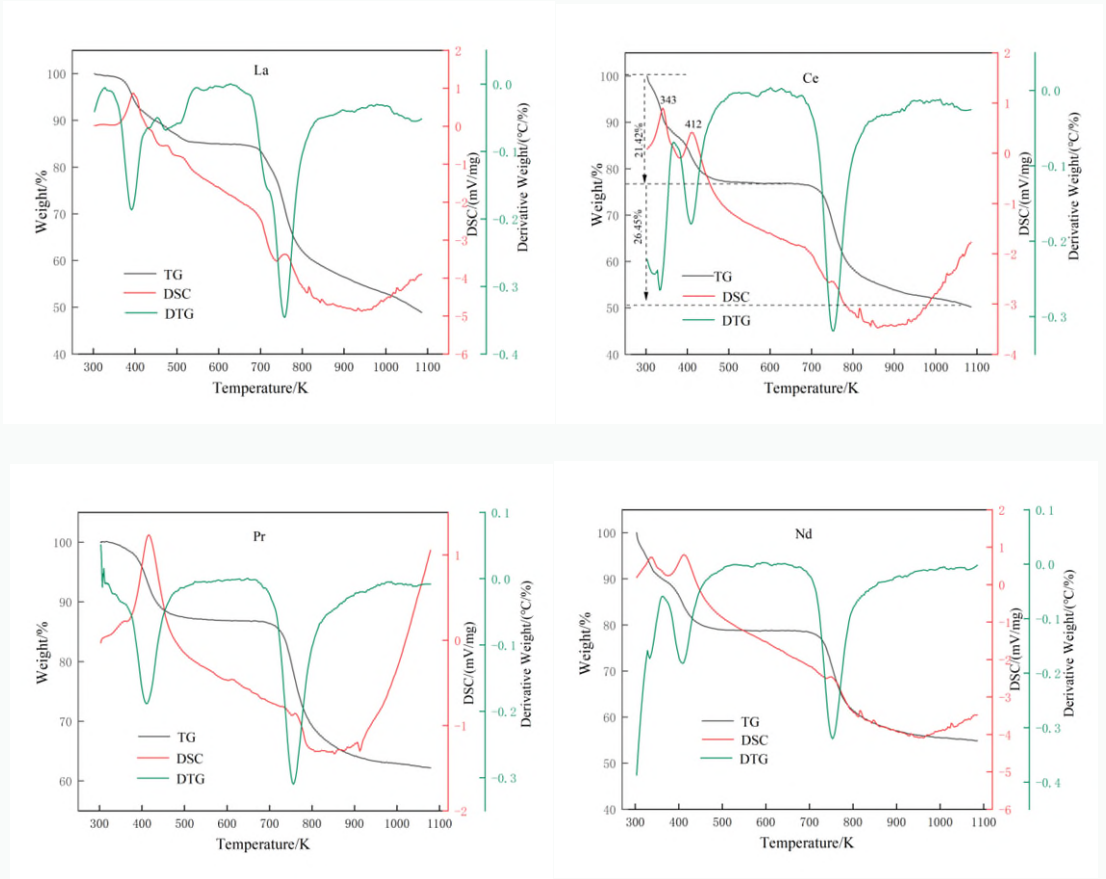


Fig. 7 The DSC-TG-DTG curves of the $[Ln_2Mn(2,6\text{-dipic})_4(H_2O)_8]\cdot 10H_2O$, Ln=La，Ce，Pr，Nd

4 CONCLUSIONS

A new family3*d*-4*f* Ln-Mn bimetallic [Ln-Mn] complexes [Ln_2Mn(2, 6-dipic)$_4$·$(H_2O)_8$]·$4H_2O$ [Ln=La, Ce, Pr, Nd,] were successfully synthesized and studied. These complexes belong to the monoclinic *C*2/*c* space group, and they were all isomorphic. The carboxyl groups O (O8, O7) of dicarboxylic acids were bridged in a bidentate cis trans manner to connect $Ln^{3+}$and Mn^{2+}. Two O 8 in two pyridine dicarboxylic acids coordinate with one $Mn^{2+}$to form a *cis-cis* carboxyl bridge conformation (-Ln^{anti}O7-O8^{syn}Mn^{syn}O8-O7^{anti}Ln-), with one Mn^{2+}at the center of the conformational chain. As a result, a *Z*-shaped chain was formed. The coordination parallel structure of pyridine-2, 6-dicarboxylic acid enhances the stability of the complexes. The results of infrared spectroscopy analysis were consistent with those of X-ray crystal analysis. The study on the thermal stability of the complex shows that it has good thermal stability. The magnetic properties of the complexes were studied, and the antiferromagnetic exchange interaction between adjacent paramagnetic ions was discovered. The magnetic data of the complexes were fitted using the Least Squares Method, and the estimated strength of the antiferromagnetic exchange interaction was obtained. At the same time, the spin orbit coupling phenomenon was explained.

SUPPLEMENTARY INFORMATION

CCDC: 2444253-2444256 contains the supplementary crystallographic data for the complexes (Ln = La (2444253), Ce(2444255), Pr (2444256), Nd(2444254), The data can be downloaded freely via http://www.ccdc.cam.ac.uk/ or from the Cambridge Crystallographic Data Centre, 12 UnionRoad, Cambridge CB2 1EZ, UK [Email: deposit@ccdc.cam.ac.uk].

Author contributions Fan Jiang: Formal analysis; Writing-original draft; Validation. Yue Ke: Formal analysis. Xiaohan Gao: Conceptualization; Formal analysis; Investigation; Writing—review & editing. Yuchi Zhou and Shuo Li: Discussion of the manuscript. Xuechuan Lv: Conceptualization; Formal analysis; Investigation; Writing—review & editing; Project administration. Almas Tusipkhan: Writing supervisor; Revised.

Acknowledgements

This work was supported by the Science and Technology Program of Liaoning Province (2025JH2/101900036) and the National Natural Science Foundation of China (Grant Nos. 21003069, 21103078). The funders had no involvement in study design, data analysis, manuscript writing or the decision to submit for publication.

Data availability No datasets were generated or analyzed during the current study.

Declarations

Competing interests The authors declare no competing interests.

References

[1] Zheng XY, Kong XJ, Long LS (2016) Synthesis and structures of lanthanide–transition metal clusters. Recent Development in Clusters of Rare Earths and Actinides: Chemistry and Materials: 51-96. https://doi.org/10.1007/430_2016_6

[2] Li, XH, Ming, Ping C, Bin Z (2013) Four coordination polymers containing 2,6-naphthalenedicarboxylic acid and 1, 10-phenanthroline: synthesis, structure, and magnetic properties. Zeitschrift für Anorganische und Allgemeine Chemie 639(3-4): 626-632. https://doi.org/10.1002/zaac.201200427

[3] Maity M, Majee MC, Kundu S, Samanta SK, Sañudo EC, Ghosh S, Chaudhury M (2015) Pentanuclear 3d–4f heterometal complexes of MII3LnIII2 (M= Ni, Cu, Zn and Ln= Nd, Gd, Tb) combinations: Syntheses, structures, magnetism, and photoluminescence properties. Inorganic Chemistry 54(20): 9715-9726. https://doi.org/10.1021/acs.inorgchem.5b01142

[4] Sharples J W, Collison D (2014) The coordination chemistry and magnetism of some 3d–4f and 4f amino-polyalcohol compounds. Coordination Chemistry Reviews 260: 1-20. https://doi.org/10.1016/j.ccr.2013.09.011

[5] Cui P, Chen Y (2016) Boratabenzene rare-earth metal complexes. Coordination Chemistry Reviews 314: 2-13. https://doi.org/10.1016/j.ccr.2015.07.014

[6] Sharples J W, Collison D (2013) Reprint of "Coordination compounds and the magnetocaloric effect". Polyhedron 66: 15-27. https://doi.org/10.1016/j.poly.2013.08.005

[7] Li ZH, Luo QC, Zheng YZ (2021) Research progress on rare earth single-molecule magnets. Chinese Journal of Rare Earth 39 (03): 391-424.

[8] Jones LF, Low DM, Helliwell M, Raftery J, Collison D, Aromí G, Cano J, Mallah T, Wernsdorfer W, Brechin EK, Mcinnes EJ (2006) Fe (III) clusters built with tripodal alcohol ligands. Polyhedron 25(2): 325-333. https://doi.org/10.1016/j.poly.2005.08.034

[9] Gamov GA, Zavalishin MN, Pimenov OA, Klochkov VV, Khodov IA (2020) La(III), Ce(III), Gd(III), and Eu(III) complexation with tris(hydroxymethyl)aminomethane in aqueous solution. Inorganic Chemistry 59(23): 17783-17793. https://doi.org/10.1021/acs.inorgchem.0c03082

[10] Ungur L, Szabo B, ALOthman ZA, Al-Kahtani AA, Chibotaru LF (2022) Mechanisms of luminescence in lanthanide complexes: A crucial role of metal-ligand covalency. Inorganic Chemistry 61(16): 5972-5976. https://doi.org/10.1021/acs.inorgchem.2c00071

[11] Li RF, Li RH, Liu XF, Chang XH, Xun F (2020) Lanthanide complexes based on a conjugated pyridine carboxylate ligand: Structures, luminescence and magnetic properties. RSC Advances 10(11): 6192-6199. https://doi.org/10.1039/c9ra10975g

[12] Orona-Návar C, Levchuk I, Moreno-Andrés J, Park Y, Mikola A, Mahlknecht J, Sillanpää M (2020) Removal of pharmaceutically active compounds (PhACs) and bacteria inactivation from urban wastewater effluents by UVA-LED photocatalysis with Gd^{3+} doped $BiVO_4$. Journal of Environmental Chemical Engineering 8(6): 10540. https://doi.org/10.1016/J.JECE.2020.104540

[13] Liu X, Zhang Y, Pan XM, Wang ZB (2023) Rare earth cerium-phenanthroline binary complex as a new corrosion inhibitor for carbon steel in acidic medium. Research on Chemical Intermediates 49(3): 1235-1257. https://doi.org/10.1007/s11164-022-04918-z

[14] Wang YJ, Jiang H, Wang HF, Mou ZH (2023) Synthesis of pyrrolidinyl-ethylene fluorenyl rare-earth metal complexes and catalysis for 2-vinylpyridine polymerization. Journal of Rare Earths 41(3): 381-387. https://doi.org/10.1016/j.jre.2022.02.018

[15] Collins J, Santoro O, Prior TJ, Chen K, Redshaw C (2021) Rare-earth metal complexes derived from the acids Ph_2C (X) CO_2H (X= OH, NH_2): Structural and ring opening polymerization (ROP) studies. Journal of

Molecular Structure 1224: 129083. https://doi.org/10.1016/j.molstruc.2020.129083

[16] Bogani L, Wernsdorfer W (2008) Molecular spintronics using single-molecule magnets. Nature materials 7(3): 179-186.https://doi.org/10.1038/nmat2133

[17] Liu K, Shi W, Cheng P (2015) Toward heterometallic single-molecule magnets: Synthetic strategy, structures and properties of 3d–4f discrete complexes. Coordination Chemistry Reviews 289: 74-122. https://doi.org/10.1016/j.ccr.2014.10.004

[18] Chen A, Dong J, Zhou K, Wang C (2017) Synthesis, crystal structure, thermal behavior and luminescence property of a cobalt (II) complex of pyridine-2, 6-dicarboxylic acid containing benzimidazole as auxiliary ligand. Molecular Crystals and Liquid Crystals 656(1): 124-130. https://doi.org/10.1080/15421406.2017.1383098

[19] Winpenny R E P (1998) The structures and magnetic properties of complexes containing 3d-and 4f-metals. Chemical Society Reviews 27(6): 447-452. https://doi.org/10.1039/A827447Z

[20] Zheng Q, Zhang TK, Wang DZ, Xu H, Li JX, Cui HH, Sun GP, Wang J (2024) Research progress on copper rare earth single-molecule magnets. Advances in Physical Chemistry 13 (3): 427-446. https://doi.org/10.12677/japc.2024.133048

[21] Fan C, Wang X, Wu X, Chen Y, Wang Z, Li M, Sun D, Tang Y, Fu G (2023) Neodymium-evoked valence electronic modulation to balance reversible oxygen electrocatalysis. Advanced Energy Materials 13(2): 2203244. https://doi.org/10.1002/aenm.202203244

[22] Zhou MF, Frenking G. (2021) Transition-metal chemistry of the heavier alkaline earth atoms Ca, Sr, and Ba. Accounts of Chemical Research 54(15): 3071-3082. https://doi.org/10.1021/acs.accounts.1c00277

[23] Huang QP, Zeng ZF, Huang QC (2020). Synthesis, crystal structure, and properties of one dimensional chain like zinc complex. Chemical Reagent 42 (10): 1207-1212. https://doi.org/10.13822/j.cnki.hxsj.2020007610

[24] Zhao Y, Cui S, Li B, Zhang J, Liu Q (2008) Structural and magnetic property of one-dimensional polymeric Ni (II) complex. Journal of Molecular Structure 873(1-3): 191-194. https://doi.org/10.1016/J.MOLSTRUC.2007.07.009

[25] Zhang C, Wei S, Sun L, Xu F, Huang P, Peng H (2018) Synthesis, structure and photocatalysis properties of two 3D Isostructural Ln (III)-MOFs based 2, 6-Pyridinedicarboxylic acid. Journal of Materials Science & Technology, 2018, 34(9): 1526-1531. https://doi.org/10.1016/J.JMST.2018.03.011

[26] Luo H (2021) Synthesis, structure, and characterization of pyridine dicarboxylic acid metal compounds. Southwest University of Science and Technology.

[27] Cui J, Li Y, Guo Z, Zheng H (2012) Six new co-coordination polymers based on a tripodal carboxylate ligand. Crystal Growth & Design 12(7): 3610-3618. https://doi.org/10.1021/CG3004323

[28] Liu B, Wei L, Li NN, Wu WP, Miao H, Wang YY, Shi QZ (2014) Solvent/temperature and dipyridyl ligands induced diverse coordination polymers based on 3-(2′, 5′-dicarboxylphenyl) pyridine. Crystal Growth & Design 14(3): 1110-1127. https://doi.org/10.1021/CG401599X

[29] Wang SJ, Lin MM, Xiong G. (2016) Structure and magnetism of three Cu (II) and Mn (II) complexes based on 3- (2,5-dicarboxyphenyl) - pyridinecarboxylic acid. Chinese Journal of Inorganic Chemistry 32 (10): 1783-1790. https://doi.org/10.11862/CJIC.20161844

[30] Liu B, Yu YH, Jiang WH, Hou GF, Gao JS (2015) A new luminescent complex constructed by oxomolybdate and 3, 5-di (4H-1, 2, 4-triazol-4-yl) benzoic acid via Mo–N bonds. Inorganic Chemistry Communications 54: 12-15. https://doi.org/10.1016/j.inoche.2015.01.034

[31] Cui SX, Zhao YL, Zhang JP, Liu Q, Zhang Y (2008) Bipyridyl second ligand dependent structural and magnetic properties of Cu (II) complexes with pyridine-2, 6-dicarboxylate and water molecule as first ligand

Crystal Growth and Design 8(10): 3803-3809. https://doi.org/10.1021/cg8004536

[32] Jeon S, Jeong Y, Ju J, Cho D, Jang YJ, Tokunaga R, Hayami S, Min KS. (2023) Synthesis, crystal structure, luminescent properties, and magnetic properties of lanthanide (III) complexes containing the chiral (S, S/R, R)-N, N'-bis (3, 5-dinitrosalicylidene)-1, 2-cyclohexanediamine ligand. Journal of Industrial and Engineering Chemistry 128: 275-285. https://doi.org/10.1016/j.jiec.2023.07.059

[33] Lustig William P, Li J. (2018) Luminescent metal‐organic frameworks and coordination polymers as alternative phosphors for energy efficient lighting devices. Coordination Chemistry Reviews 373: 116-147. https://doi.org/10.1016/j.ccr.2017.09.017

[34] Gong TT, Yang S, Wang ZX, Li MY, Zhang SY, Liu JC, Chen LJ, Zhao JW (2023) Dual-ligand-functionalized dodeca-nuclear lanthanide–tungsten-cluster incorporated selenotungstates and fluorescence detection of dipicolinic acid. Inorganic Chemistry Frontiers 10(9): 2799-2810. https://doi.org/10.1039/d3qi00361b

[35] Kim J, Lim JM, Suh MC, Yun H (2001) Crystal structure and magnetic properties of dicarboxylate-bridged linear chain Mn (II) complexes. Polyhedron 20(15-16): 1947-1951. https://doi.org/10.1016/S0277-5387(01)00791-4

[36] Deniz M, Pasan J, Ferrando-Soria J (2011) Synthesis, structural analysis, and magnetic properties of ethylmalonate-manganese (II) complexes. Inorganic Chemistry 50(21): 10765-10776. https://doi.org/10.1021/ic201314k

[37] F. E. Mabbs, D. J. Machin (1973) Magnetism and transition metal complexes. Chapman and Hall; U.S.A. Halsted Press, New York. https://doi.org/10.1016/0022-2860(74)85025-8

[38] Rabu P, Rueff JM, Huang ZL, Angelov S, Souletie J, Drillon M (2001) Copper (II) and cobalt (II) dicarboxylate-based layered magnets: influence of π electron ligands on the long range magnetic ordering. Polyhedron 20(11-14): 1677-1685. https://doi.org/10.1016/S0277-5387(01)00672-6

[39] Zou HH, Zhang SH, Zeng MH, Zhou YL, Liang H (2008) Crystal structure and magnetic properties of a unique 3D coordination polymer constructed from flexible aliphatic tricarballylic acid ligands featuring linear trimeric Manganese (II)-based, metal carboxylate chains. Journal of Molecular Structure 885(1-3): 50-55. https://doi.org/10.1016/j.molstruc.2007.10.009

[40] Rueff JM, Masciocchi N, Rabu P, Sironi A, Skoulios A. (2002) Synthesis, structure and magnetism of homologous series of polycrystalline cobalt alkane mono-and dicarboxylate soaps. Chemistry–A European Journal 8(8): 1813-1820. https://doi.org/10.1002/1521-3765(20020415)8:8<1813::aid-chem1813>3.0.co;2-g

[41] Chang JH, Dong QG. (2006) Spectrum Principles and Analysis (in Chinese), Science Press, Beijing, pp 88-91.

Supplementary Files

This is a list of supplementary files associated with this preprint. Click to download.

- Supplementarydata.docx
- GraphicAbstract.doc